where μ is the Lyapunov exponent of the single-patch map F on the associated single patch trajectory and the λ_k are the eigenvalues of M.

24. J. A. J. Metz, R. M. Nisbet, S. A. H. Geritz, *Trends Ecol. Evol.* **7**, 198 (1992).
25. In this note, we sketch some of the key ideas involved in establishing criteria 1, 2, and 3. Mathematical details are given elsewhere (*42*). Trajectories of the single-patch map are coherent solutions (*16*) of the corresponding metapopulation if and only if $(1, 1, \ldots, 1)$ is an eigenvector of M with eigenvalue 1; we assume this because we are interested in spatial generalizations of nonspatial population models. Locally (in phase space), the system will relax to coherence if all but the maximum Lyapunov exponent are negative; thus, we require (*23*)
$$\mu + \log|\lambda| < 0 \quad (11)$$
where λ is the subdominant (*22*) eigenvalue of M. This is criterion 1. (To obtain the boundaries of the blue regions in Fig. 1, we approximated Eq. 9 with a finite sum.) A few special cases of this local result (for particular types of matrices M) have been noted previously (*26–30*). All these previous results are subsumed by criterion 1. From Eq. 9, it is clear that if $r = \sup_x|F'(x)|$, then $\mu(x^0) \leq \log r$ regardless of the initial condition x^0. Consequently
$$\log r + \log|\lambda| < 0 \quad (12)$$
is sufficient to guarantee that the system relaxes to coherence globally (in phase space). This is criterion 3. In general, more than one coherent solution of Eqs. 5 may be locally stable, so different initial states may be attracted to different coherent solutions. If the single-patch map always has a unique attractor [which is true, in particular, for the logistic map (*40*)], then condition 3 guarantees that the corresponding coherent attractor of the metapopulation is the unique attracting solution of Eqs. 5. Both the local and global coherence criteria can be established rigorously and do not depend on M being diagonalizable; elsewhere (*42*), we show this in detail and rigorously characterize the dispersal patterns of systems that admit locally stable coherent oscillations (in practice, this includes all ecologically relevant models).
26. K. Kaneko, *Phys. Rev. Lett.* **63**, 219 (1989).
27. A. Hastings, *Ecology* **74**, 1362 (1993).
28. R. V. Solé, J. G. P. Gamarra, *J. Theor. Biol.* **193**, 539 (1998).
29. J. A. L. Silva, M. L. De Castro, D. A. R. Justo, *Bull. Math. Biol.* **62**, 337 (2000).
30. T. Bohr, M. H. Jensen, G. Paladin, A. Vulpiani, *Dynamical Systems Approach to Turbulence* (Cambridge Univ. Press, Cambridge, 1998), §4.1.1.
31. The logistic metapopulation model that we used for the figures is merely the simplest idealized case. However, the results for the logistic reproduction function are representative for many systems (the sequence of bifurcations is generic in a broad class of dynamical systems). In addition, simulations show that our results are not substantially affected by demographic or environmental stochasticity (local noise).
32. Our analytical results, Eqs. 1 to 3, can be generalized in a number of important ways (*42*). They apply, essentially as stated, to metapopulations involving multiple species, age structure, external (explicitly time-dependent) forcing, and other realistic features. The key technical point behind these extensions is that our derivations of the coherence conditions do not depend on the single-patch map (F) being one-dimensional. If F is multidimensional, then in the local criteria 1 and 2, the Lyapunov exponent μ is simply replaced by the maximal Lyapunov exponent of the multidimensional single-patch map; in the global criterion 3, the maximum reproductive rate [$r = \sup_x|F'(x)|$] is replaced by the maximum of the matrix norm of the Jacobian derivative of F. Similar conditions can also been obtained for systems involving continuous space and/or continuous time.
33. It is an immediate consequence of condition 1 that locally stable, nonchaotic solutions of the single-patch map are always locally stable as coherent solutions (*16*) of the metapopulation. The reason is that $|\lambda| < 1$ for any ecological model (*42*) and $\mu \leq 0$ for nonchaotic dynamics (equilibria, cycles, or quasi-periodic oscillations), so condition 1 always holds. For coherent chaos, local stability depends on the dispersal pattern. For any given $\mu > 0$, there are dispersal matrices such that $e^{\mu}|\lambda| < 1$ and others such that $e^{\mu}|\lambda| > 1$. In Fig. 1, we see that (for the logistic metapopulation with equal coupling) if the fraction of dispersing individuals (m) is sufficiently large, then coherent solutions are always locally stable, even at the extreme of $r = 4$.
34. A. Hastings, C. L. Hom, S. Ellner, P. Turchin, H. C. Godfray, *Annu. Rev. Ecol. Syst.* **24**, 1 (1993).
35. S. Ellner, P. Turchin, *Am. Nat.* **145**, 343 (1995).
36. The subdominant (*22*) eigenvalue λ is a function only of the dispersal matrix M, not the within-patch map F. Consequently, even if we cannot obtain any reasonable approximation of F for a real system, we can use estimates of changes in λ to predict roughly how conservation measures such as corridors affect coherence (and extinction) probabilities. Small changes in λ typically do not yield large changes in the total volume of the basins of attraction of coherent oscillations.
37. R. M. Anderson, R. M. May, *Infectious Diseases of Humans: Dynamics and Control* (Oxford Univ. Press, Oxford, 1991).
38. D. J. D. Earn, P. Rohani, B. M. Bolker, B. T. Grenfell, *Science* **287**, 667 (2000).
39. R. M. May, *Nature* **261**, 459 (1976).
40. P. Collet, J.-P. Eckmann, *Iterated Maps on the Interval as Dynamical Systems*, vol. 1 of *Progress in Physics* (Birkhäuser, Basel, 1980).
41. J. Guckenheimer, P. Holmes, *Nonlinear Oscillations, Dynamical Systems, and Bifurcations of Vector Fields*, vol. 42 of *Applied Mathematical Sciences* (Springer-Verlag, Berlin, 1983).
42. D. J. D. Earn, S. A. Levin, in preparation.
43. A. Hastings, K. Higgins, *Science* **263**, 1133 (1994).
44. We thank A. Balmford, S. Balshine, B. Grenfell, R. Johnstone, L. Stone, and L. Worden for helpful discussions and comments on a preliminary manuscript. We were supported by the Natural Sciences and Engineering Research Council of Canada (NSERC), the Royal Society, the Sloan Foundation, and the David and Lucile Packard Foundation (award number 8910-48190).

20 June 2000; accepted 3 October 2000

PSD-95 Involvement in Maturation of Excitatory Synapses

Alaa El-Din El-Husseini,[1]* Eric Schnell,[2]* Dane M. Chetkovich,[1,3] Roger A. Nicoll,[2] David S. Bredt[1]†

PSD-95 is a neuronal PDZ protein that associates with receptors and cytoskeletal elements at synapses, but whose function is uncertain. We found that overexpression of PSD-95 in hippocampal neurons can drive maturation of glutamatergic synapses. PSD-95 expression enhanced postsynaptic clustering and activity of glutamate receptors. Postsynaptic expression of PSD-95 also enhanced maturation of the presynaptic terminal. These effects required synaptic clustering of PSD-95 but did not rely on its guanylate kinase domain. PSD-95 expression also increased the number and size of dendritic spines. These results demonstrate that PSD-95 can orchestrate synaptic development and are suggestive of roles for PSD-95 in synapse stabilization and plasticity.

Despite the central role for synapses in neuronal function, mechanisms underlying synapse formation remain incompletely understood. Recently, proteins containing PDZ motifs have been proposed as molecular scaffolds for receptors and cytoskeletal elements at synapses (*1–4*). The prototypical PDZ protein, postsynaptic density–95 (PSD-95/SAP-90), is a membrane-associated guanylate kinase (MAGUK) concentrated at glutamatergic synapses (*5*, *6*). PSD-95 may participate in synapse development because it clusters at synapses before other postsynaptic proteins (*7*), and because *discs large*, a PSD-95 homolog in *Drosophila*, is necessary for proper development of larval neuromuscular junctions (*8*). Despite numerous studies it remains uncertain whether PSD-95 participates in synapse development in mammals. Targeted disruption of PSD-95 in mice does not alter synaptic structure (*9*), possibly because three other MAGUKs and dozens of other PDZ proteins occur at brain synapses. This molecular redundancy has obscured understanding of functions for PSD-95 and other PDZ proteins in the brain.

We overexpressed PSD-95 to help define its roles (*10*). Green fluorescent protein (GFP)–tagged versions of PSD-95 target faithfully to postsynaptic sites in hippocampal neurons, despite being overexpressed 5 to 10 times above endogenous levels (*11*, *12*). To evaluate the effects of PSD-95 on synaptic development, we analyzed cultures at early developmental stages, day in vitro (DIV) 10 to 12, and noted an increase of glutamate receptor subunit–1 (GluR1) immunofluorescence at postsynap-

[1]Department of Physiology, [2]Department of Cellular and Molecular Pharmacology, and [3]Department of Neurology, University of California, San Francisco 94143, USA.

*These authors contributed equally to this work.
†To whom correspondence should be addressed: E-mail: bredt@itsa.ucsf.edu

tic sites of neurons transfected for PSD-95 (Fig. 1A). This increase was detected both in permeabilized cells with an antibody to a cytosolic GluR1 epitope (Fig. 1A) and in live cells with an antibody to an extracellular site (*13*). When compared with neighboring untransfected cells, neurons overexpressing PSD-95 exhibited synaptic GluR1 labeling ~250% of control. By contrast, PSD-95 overexpression did not alter synaptic clustering of *N*-methyl-D-aspartate (NMDA) receptor–1 (NR1) (Fig. 1B). These results are surprising because PSD-95 directly binds to NMDA receptors (NMDARs) but not to GluRs (*1*, *3*). This suggests that PSD-95 may have an unexpected role in synaptic assembly.

We wondered whether these postsynaptic effects of PSD-95 overexpression occur in both excitatory pyramidal neurons and inhibitory interneurons. Glutamic acid decarboxylase (GAD)–negative pyramidal neurons had a punctate distribution for PSD-95 and GluR1 at spiny protrusions of the dendritic membrane, whereas the GAD-positive interneurons showed more linear clustering along the dendritic shaft (Fig. 1, C and D). Quantitating the intensity of synaptic staining showed that PSD-95 transfection selectively enhanced GluR1 clustering in both pyramidal cells and interneurons (Fig. 1, D and E) and the synaptic GluR1 fluorescence intensity correlated with the PSD-95 expression (*13*). Overexpression of other postsynaptic proteins, including Ca^{2+}/calmodulin-dependent protein kinase II (CaMKII) and nNOS, did not affect GluR1 clustering (*13*).

To determine whether this PSD-95–mediated enhancement of GluR1 clustering augments postsynaptic function, we measured miniature excitatory postsynaptic currents (mEPSCs) (*14*). Each recorded cell was identified as excitatory or inhibitory by injecting with Lucifer yellow and double labeling for GAD-65 (Fig. 2A). GAD-positive interneurons in our cultures had larger and more numerous mEPSCs than GAD-negative pyramidal neurons (Fig. 2, B_1 and C_1), consistent with differences in GluR1 clustering detected anatomically (Fig. 1C). For both pyramidal cells and interneurons, transfection with PSD-95 augmented the amplitude of mEPSCs, indicating that the additional GluRs recruited by PSD-95 are functional (Fig. 2, B and C). The frequency of mEPSCs was also enhanced by PSD-95 transfection (Fig. 2, B to E).

Changes in mEPSC frequency generally reflect presynaptic effects (*15*); we therefore assessed whether postsynaptic expression of PSD-95 might alter the presynaptic terminal. Staining for synaptophysin and synaptic vesicle protein 2 (SV-2) was enhanced in axon terminals contacting postsynaptic sites of PSD-95–transfected pyramidal cells (synaptophysin density = 257 ± 35% of control; SV-2 = 245 ± 24% of control) [Fig. 3, A and D (*13*)], as well as interneurons (synaptophysin density = 203 ± 6% of control). We also labeled transfected cultures with FM4-64, which marks sites of synaptic vesicle endocytosis (*16*). Labeling by FM4-64 was markedly enhanced at presynaptic sites that oppose postsynaptic sites labeled by PSD-95–GFP (FM4-64 intensity = 184 ± 17% of control) (Fig. 3B), suggesting a larger presynaptic vesicle pool size and supporting our physiological data of increased presynaptic release (Fig. 2).

Does the enhancement of synaptic function by PSD-95 require its targeting to synaptic sites? We transfected neurons with a PSD-95 mutant (PSD-95:C3,5S) lacking NH_2-terminal palmitoylation, which is required for synaptic clustering (*11*). PSD-95:C3,5S occurred diffusely in hippocampal neurons (Fig. 3C). It did not enhance GluR1 clustering but instead partially disrupted GluR1 clustering in pyramidal cells (Fig. 3, C and D). Neurons transfected with this mutant also failed to display augmented mEPSC amplitude and frequency {untransfected: amplitude = 9.14 ± 0.37 pA, frequency = 1.57 ±

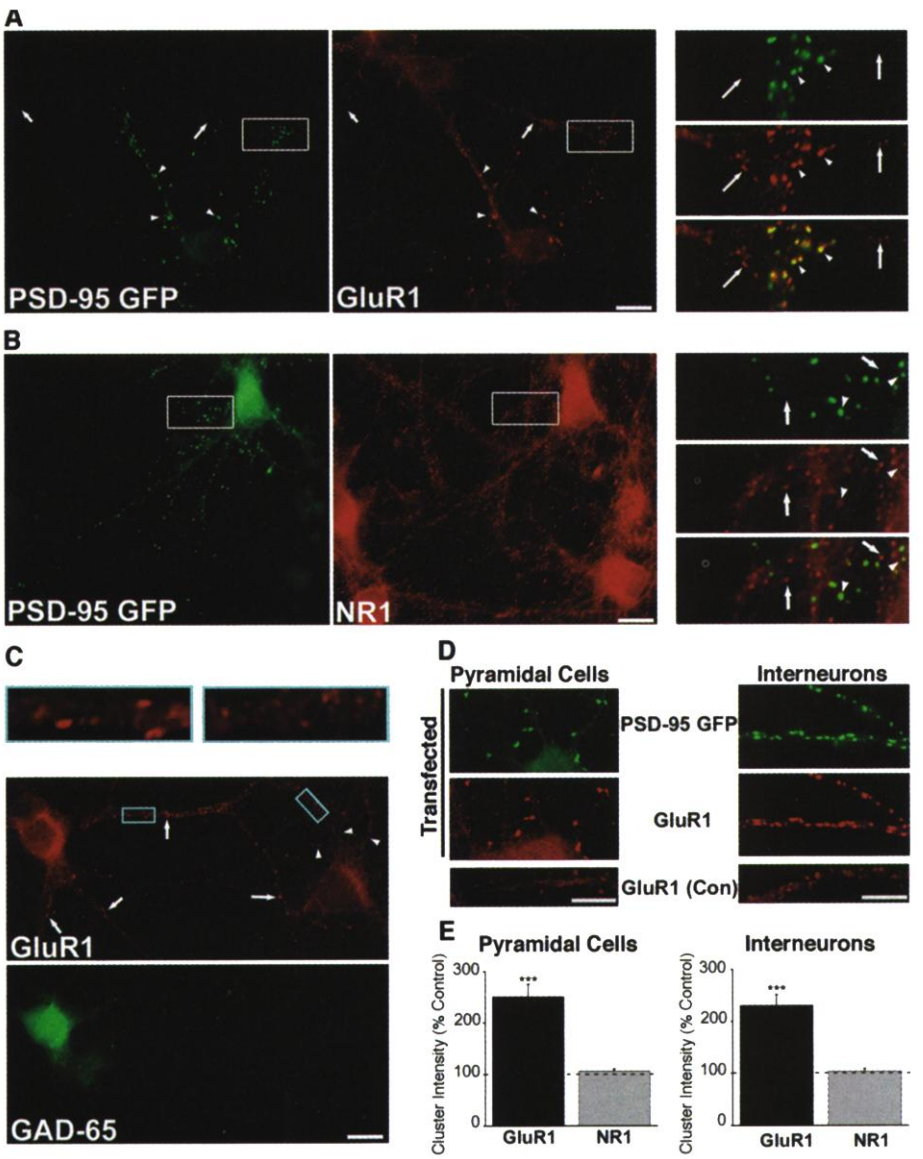

Fig. 1. Expression of PSD-95 enhances synaptic clustering of AMPA but not NMDA receptors. (**A**) Hippocampal neurons were transfected with PSD-95–GFP, fixed at DIV 12, and stained for GluR1 or NR1. Higher magnification micrographs of the boxed regions are shown in the panels to the right. Clusters of GluR1 are more intense in spines from the neuron transfected with PSD-95 (arrowheads) than in spines from the neighboring untransfected neuron (arrows). (**B**) NR1 staining is equally intense in spines from transfected (arrowheads) and untransfected (arrows) neurons. (**C**) GluR1 shows spiny clusters (arrowheads) in GAD-negative pyramidal cells and forms shaft clusters (arrows) in GAD-positive interneurons. (**D** and **E**) GluR1 clustering is selectively enhanced both in pyramidal cells and in interneurons overexpressing PSD-95–GFP, whereas NR1 is not. ***$P <$ 0.001. Scale bars, 10 μm.

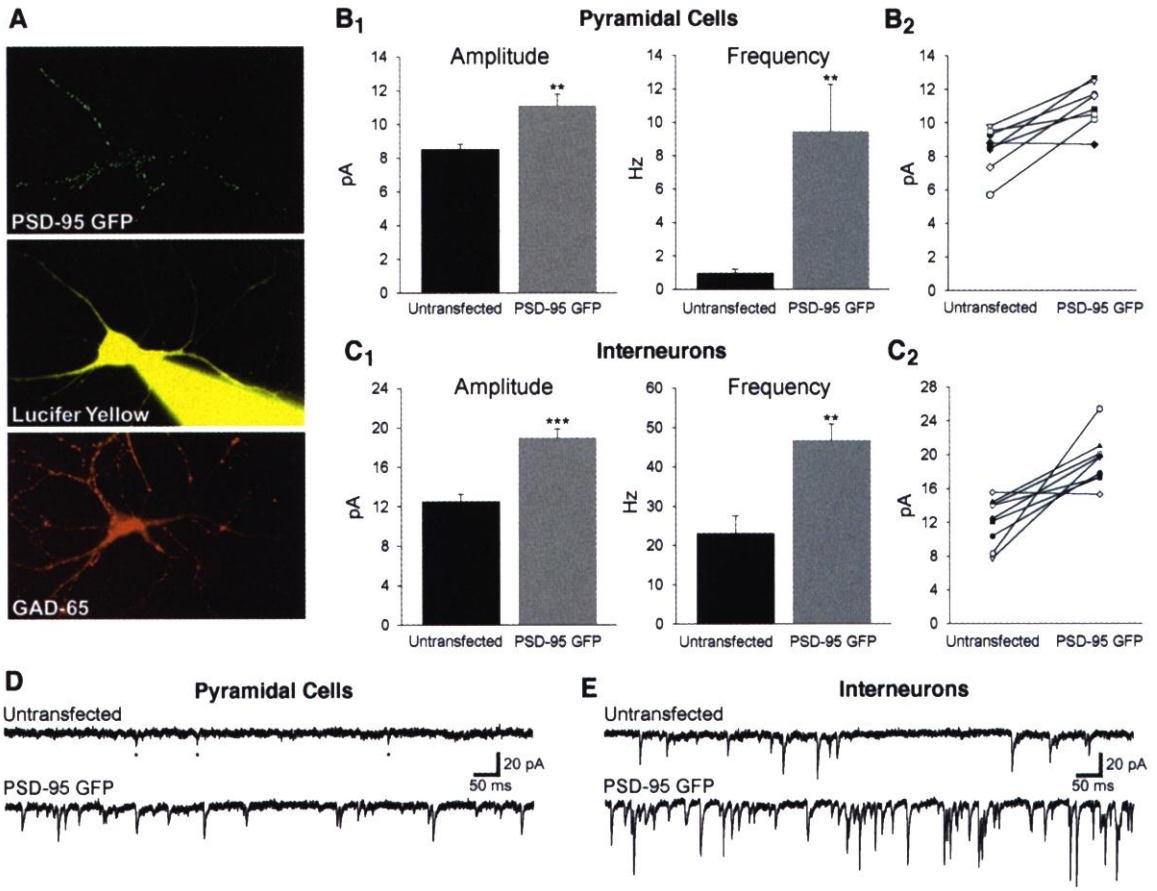

Fig. 2. PSD-95 overexpression increases the amplitude and frequency of AMPA receptor–mediated miniature synaptic currents. (**A**) To determine neurotransmitter phenotypes for all PSD-95–GFP–transfected and –untransfected cells, Lucifer yellow was injected during recording, and cultures were later stained for GAD-65, which identifies this cell as an inhibitory interneuron. Both PSD-95–overexpressing pyramidal cells (**B**) (n = 16, 13) and interneurons (**C**) (n = 19, 10) show increased mEPSC amplitudes and frequencies (**P < 0.01, ***P < 0.001). PSD-95–transfected cells have increased mEPSC amplitude when compared with neighboring untransfected cells for both pyramidal cells (B_2, n = 8 pairs) and interneurons (C_2, n = 9 pairs). (**D** and **E**) Current traces from neighboring untransfected (top) and PSD-95–GFP–expressing (bottom) pyramidal cells (D) and interneurons (E). mEPSCs in untransfected pyramidal cells are marked with an asterisk.

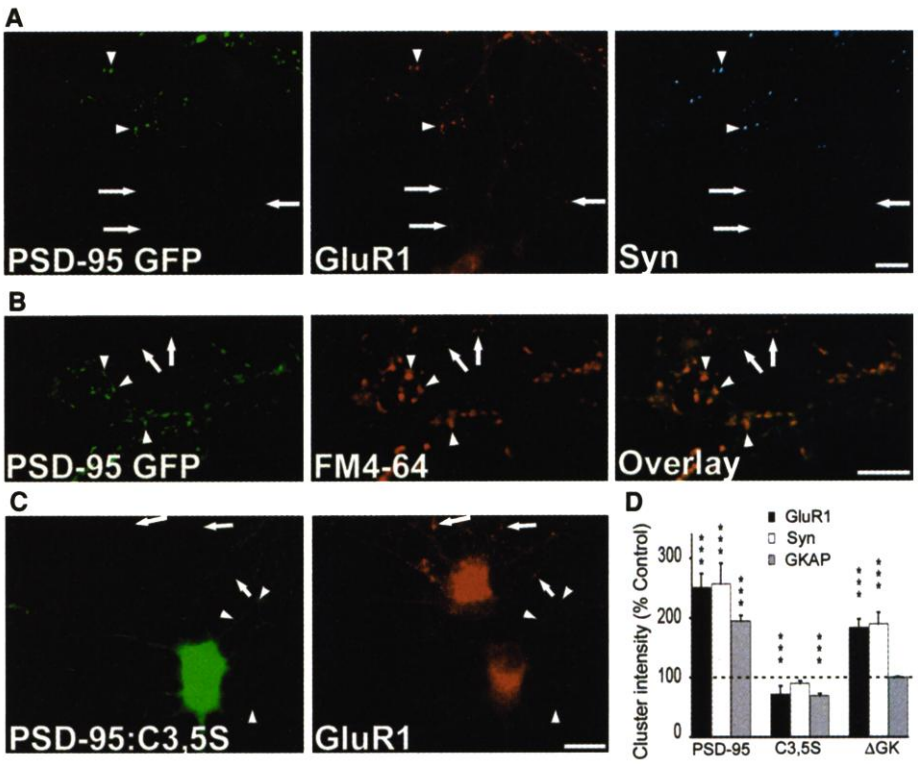

Fig. 3. Postsynaptic expression of PSD-95 enhances presynaptic development. (**A**) PSD-95–GFP–transfected hippocampal neurons were fixed at DIV 10 and stained for GluR1 and synaptophysin. At synapses onto neurons transfected with PSD-95 (arrowheads), both GluR1 and synaptophysin (Syn) staining are more intense than at synapses onto untransfected neurons (arrows). (**B**) Hippocampal neurons transfected with PSD-95–GFP and incubated with 15 μM FM4-64 in the presence of 90 mM KCl for 45 s show enhanced staining of FM4-64 at sites opposing PSD-95–GFP clusters (arrowheads) than at untransfected synapses (arrows). (**C**) Expression of the palmitoylation-deficient mutant form of PSD-95 (PSD-95:C3,5S) reduces clustering of GluR1. (**D**) Quantitative analysis of synaptic changes resulting from PSD-95, PSD-95:C3,5S (C3,5S), and PSD-95ΔGK transfections (***P < 0.001). Scale bars, 10 μm.

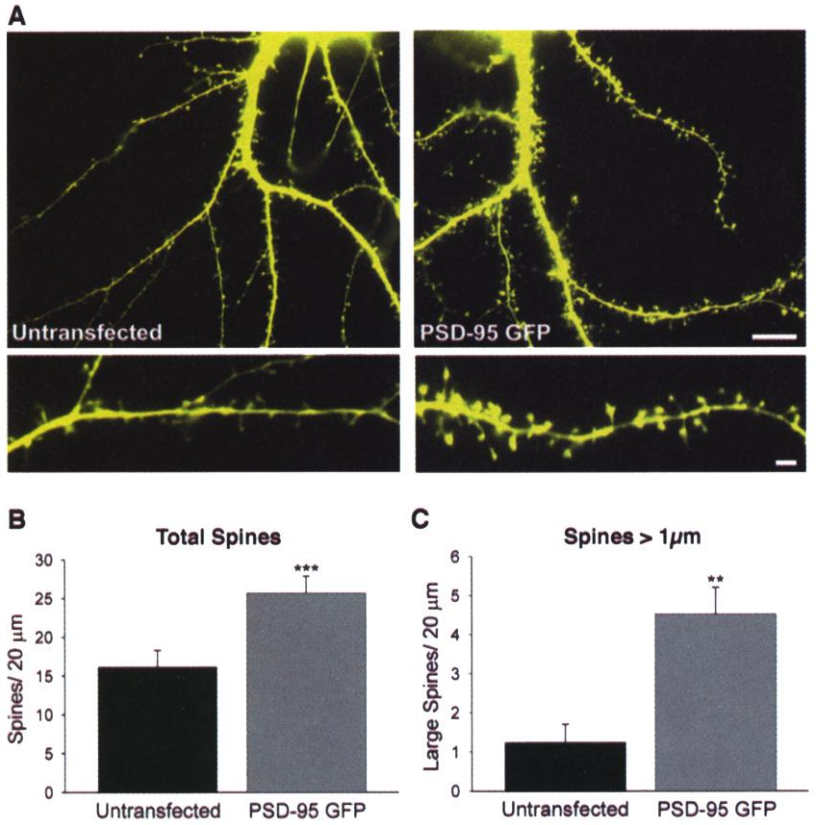

Fig. 4. PSD-95 overexpression enhances spine maturation. Hippocampal neurons (DIV 21) expressing PSD-95–GFP were filled with Lucifer yellow, fixed, and analyzed for number and size of spines. Nearby untransfected cells were chosen randomly and filled as controls. (**A**) Two filled pyramidal cells from the same coverslip demonstrate the increased spine size and density in the transfected cells. Scale bars, 10 μm (upper), 2 μm (lower). (**B**) The density of spines was augmented in cells expressing PSD-95–GFP (n = 17 each). (**C**) Neurons expressing PSD-95–GFP showed an increased density of spines >1 μm in diameter. $^{**}P < 0.01$, $^{***}P < 0.001$.

1.00 Hz; PSD-95:C3,5S: amplitude = 8.60 ± 0.60 pA [not significant (NS), P = 0.4], frequency = 0.79 ± 0.24 Hz [NS, P = 0.44]}. The palmitoylation-deficient mutant of PSD-95 thus failed to enhance GluR1 clustering or presynaptic maturation and may function as a partially dominant-interfering mutant.

Overexpression of PSD-95 also augmented postsynaptic clustering of a PSD-95–associated protein, guanylate kinase associated protein (GKAP) (*17*), but clustering of a noninteracting protein, CaMKII, was not affected (*13*). We wondered whether the increase in synaptic GKAP might mediate enhanced GluR clustering by PSD-95, because GKAP binds to an actin-associated postsynaptic complex containing Shank (*18*). However, neurons transfected with PSD-95 lacking the GK domain still showed enhanced postsynaptic clustering of GluR1 and presynaptic aggregation of synaptophysin in the absence of augmented GKAP clustering (*13*) (Fig. 3D). The GKAP-Shank complex does not, therefore, appear to be necessary for enhanced synaptic development by PSD-95.

Given that PSD-95 enhances a number of pre- and postsynaptic markers at early developmental stages, we wondered if there might be associated morphological changes at later stages. We therefore allowed neurons to develop in culture for 3 weeks, filled them with Lucifer yellow, and compared the morphology of transfected cells with that of their neighbors. Dendritic spines detected in PSD-95–transfected neurons were both more numerous and larger than those in untransfected neurons (Fig. 4). The modest increase in spine count may have resulted from a proliferation of spines or from the inclusion of enlarged spines that would otherwise have been undetectable. Most notable was the increased density of large spines >1 μm in diameter (Fig. 4C).

PSD-95 can drive maturation of synapses, not only of postsynaptic components but also of presynaptic terminals. The selective enhancement of GluR1 versus NR1 clustering correlates with previous anatomical studies showing that the number of NMDARs remains relatively constant, whereas the number of synaptic GluRs increases during development (*19*, *20*) and the magnitude of GluR quantal response increases as synapses mature (*21*). It is not clear whether the increase in size of synaptic spines and the increase in GluR1 clustering induced by PSD-95 are parallel processes or if one triggers the other (*22*). Also unclear is the mechanism underlying the enhanced GluR1 clustering, which presumably involves an intermediary protein(s), because PSD-95 does not bind GluR1 (*23*).

The enhanced size of axon terminals contacting neurons transfected with PSD-95 and the increased frequency of mEPSCs can be explained by the hypothesis that PSD-95 conveys a retrograde signal for presynaptic development. The increased frequency of mEPSCs presumably reflects the increased probability of release associated with an increased vesicle pool size (*24*). This result may explain why the PSD-95 knockout mouse has augmented paired pulse facilitation (*9*), which would be consistent with a decreased probability of release in the mutant. The transsynaptic influence of PSD-95 is reminiscent of rapsyn, a nicotinic acetylcholine receptor clustering protein essential for differentiation of motor neuron terminals (*25*). PSD-95 may communicate with the axon through neuroligin, a PSD-95–associated cell adhesion molecule that links to the nerve terminal by means of neurexins (*26*, *27*). Very recent studies show that neuroligin expression in heterologous cells can trigger presynaptic development (*28*).

In addition to sculpting developing synapses, PSD-95 may contribute to synapse stabilization and remodeling in adult brain (*29*). Targeted disruption of PSD-95 alters activity-dependent synaptic plasticity and learning (*9*). Because PSD-95 clustering is controlled by its PDZ domains, palmitoylation, and intramolecular SH3/GK domain interaction (*11*, *30*, *31*), it will be of interest to determine whether these sites are regulated by neural activity to modulate synaptic structure and plasticity.

References and Notes

1. S. H. Lee, M. Sheng, *Curr. Opin. Neurobiol.* **10**, 125 (2000).
2. S. E. Craven, D. S. Bredt, *Cell* **93**, 495 (1998).
3. M. B. Kennedy, *Brain Res. Brain Res. Rev.* **26**, 243 (1998).
4. C. C. Garner, J. Nash, R. L. Huganir, *Trends Cell Biol.* **10**, 274 (2000).
5. K. O. Cho, C. A. Hunt, M. B. Kennedy, *Neuron* **9**, 929 (1992).
6. U. Kistner *et al.*, *J. Biol. Chem.* **268**, 4580 (1993).
7. A. Rao, E. Kim, M. Sheng, A. M. Craig, *J. Neurosci.* **18**, 1217 (1998).
8. T. Lahey, M. Gorczyca, X. X. Jia, V. Budnik, *Neuron* **13**, 823 (1994).
9. M. Migaud *et al.*, *Nature* **396**, 433 (1998).
10. Low-density hippocampal cultures (5 × 10^4 cells/cm^2) were transfected and maintained as described (*11*) and then stained by immunofluorescence with the following antibodies: rabbit polyclonal antibodies to PSD-95 (*32*), CaMKII, GluR1, synaptophysin, GKAP (*17*), and GAD-65 (gift from S. Baekkeskov), and mouse monoclonal antibodies to NR1, synaptophysin, SV-2, PSD-95, and GFP. Quantification of protein clustering in dendrites was performed on 10 to 20 neurons from two or three independent transfec-

tions. Images of neurons were acquired with a charge-coupled device camera with a 60× oil-immersion objective (numerical aperture = 1.4) affixed to an inverted microscope and quantitated with Metamorph imaging software. For each neuron studied, the three largest caliber proximal dendrites (~20 μm long) were analyzed. To quantitate changes in clustering, we measured the average pixel intensities of all synaptic clusters along these dendritic segments in transfected and neighboring nontransfected cells and analyzed data by paired *t* test. All clusters that colocalized with synaptophysin and were at least twice the background intensity were analyzed.

11. S. E. Craven, A. E. Husseini, D. S. Bredt, *Neuron* **22**, 497 (1999).
12. D. B. Arnold, D. E. Clapham, *Neuron* **23**, 149 (1999).
13. Supplementary figures are available at *Science* Online at www.sciencemag.org/cgi/content/full/290/5495/1364/DC1.
14. Whole-cell recordings were made at room temperature from 11- to 13-day-old cultured neurons, with 4- to 6-megohm patch pipettes. Pipette solutions contained (in mM) 94 Cs-gluconate, 2 CsCl, 8 tetraethylammonium-Cl, 4 QX-314Cl, 7 NaCl, 8 Hepes, 0.2 EGTA, 3 MgATP, 0.3 Na_3GTP, and 0.02 to 0.1% Lucifer yellow CH. Cultures were continuously superfused with buffer containing (in mM) 112 NaCl, 3 KCl, 16 glucose, 8 Hepes, 2 $CaCl_2$, 2 $MgCl_2$, 0.1 picrotoxin, and 0.001 tetrodotoxin at 1 ml/min. Cells were patched under visual guidance with a water-immersion microscope. Transfected cells were identified before recording by fluorescence. Current records were low-pass filtered at 2 kHz, stored on tape, and digitized off-line at 5 kHz. Cells were held at −70 mV, and recording stability was monitored in real time with −4-mV steps every 10 s. Series resistances ranged between 15 and 25 megohm. Recordings were made for 2 to 10 min from each cell, depending on mEPSC frequency (cells with higher frequencies were recorded for less time). mEPSCs were analyzed with customized software (E. Schnell), with an amplitude threshold of 5 pA. To control for variability, neighboring transfected and untransfected cells were selected for recording. Transfected and untransfected cells were compared with the unpaired *t* test. To assess spine morphology, 21 or 22 DIV neurons were filled with 0.1% Lucifer yellow for 3 min, fixed in paraformaldehyde, and stained for GAD-65 to exclude interneurons. Images were taken with a 100× oil-immersion objective, and an observer blinded with respect to neuronal transfection quantitated spine size and density.
15. Although increases in mEPSC frequency typically reflect increased probability of transmitter release, an enlarged mEPSC amplitude can also increase apparent frequency, because very small events can be amplified to the detection threshold. To determine whether a change in mEPSC detection might account for the increase in frequency, we made additional recordings from cultured neurons at different holding potentials to manipulate mEPSC amplitude. In these experiments, an increase of mEPSC amplitude that corresponded to the observed difference between untransfected and PSD-95–transfected pyramidal cells (from 8.4 ± 0.3 pA to 11.4 ± 0.2 pA, $n = 4$) was associated with a 2.9 ± 0.6–fold increase in the mEPSC frequency. Because the transfected neurons had a 9.8 ± 2.9–fold greater mEPSC frequency, the change in mEPSC detection is unable to account for the increase in frequency, confirming that a change in presynaptic function has occurred.
16. A. J. Cochilla, J. K. Angleson, W. J. Betz, *Annu. Rev. Neurosci.* **22**, 1 (1999).
17. E. Kim *et al.*, *J. Cell Biol.* **136**, 669 (1997).
18. S. Naisbitt *et al.*, *Neuron* **23**, 569 (1999).
19. Z. Nusser *et al.*, *Neuron* **21**, 545 (1998).
20. R. S. Petralia *et al.*, *Nature Neurosci.* **2**, 31 (1999).
21. S. N. Gomperts, R. Carroll, R. C. Malenka, R. A. Nicoll, *J. Neurosci.* **20**, 229 (2000).
22. R. A. McKinney, M. Capogna, R. Dürr, B. H. Gähwiler, S. M. Thompson, *Nature Neurosci.* **2**, 44 (1999).
23. A. S. Leonard, M. A. Davare, M. C. Horne, C. C. Garner, J. W. Hell, *J. Biol. Chem.* **273**, 19518 (1998).
24. An increase in mEPSC frequency can result from an increase in the probability of transmitter release from an individual synapse and/or from an increase in the number of synapses. It has been reported that the probability of release is related to the size of the vesicle pool (33). Given the lack of change in the number of synapses contacting PSD-95–transfected cells in DIV 12 neurons (untransfected: GluR1 puncta = 0.614 ± 0.054 μm^{-1}; PSD-95–GFP: GluR1 puncta = 0.714 ± 0.054 μm^{-1}; $P > 0.05$), we conclude that much of the change is due to an increase in release probability secondary to the larger vesicle pool implied by the enhanced synaptophysin and FM4-46 staining.
25. M. Gautam *et al.*, *Nature* **377**, 232 (1995).
26. M. Irie *et al.*, *Science* **277**, 1511 (1997).
27. K. Ichtchenko *et al.*, *Cell* **81**, 435 (1995).
28. P. Scheiffele, J. Fan, J. Chioh, R. Fetter, T. Serafini, *Cell* **101**, 657 (2000).
29. M. Maletic-Savatic, R. Malinow, K. Svoboda, *Science* **283**, 1923 (1999).
30. A. W. McGee, D. S. Bredt, *J. Biol. Chem.* **274**, 17431 (1999).
31. H. Shin, Y. P. Hsueh, F. C. Yang, E. Kim, M. Sheng, *J. Neurosci.* **20**, 3580 (2000).
32. J. E. Brenman, K. S. Christopherson, S. E. Craven, A. W. McGee, D. S. Bredt, *J. Neurosci.* **16**, 7407 (1996).
33. V. N. Murthy, T. J. Sejnowski, C. F. Stevens, *Neuron* **18**, 599 (1997).
34. We thank R. Edwards, M. von Zastrow, and G. Davis for critical reviews of earlier versions of the manuscript. Supported by grants from the NIH (R.A.N. and D.S.B.), Howard Hughes Medical Institute Research Resources Program (D.S.B.), and Human Frontier Research Program (D.S.B.). D.M.C. is a postdoctoral fellow of the Howard Hughes Medical Institute, A.E-D.E.-H. is supported by a grant from the Medical Research Council of Canada and E.S. is supported by the Medical Scientist Training Program.

19 July 2000; accepted 20 October 2000

Intracellular Parasitism by *Histoplasma capsulatum*: Fungal Virulence and Calcium Dependence

Tricia Schurtz Sebghati, Jacquelyn T. Engle, William E. Goldman*

Histoplasma capsulatum **is an effective intracellular parasite of macrophages and causes the most prevalent fungal respiratory disease in the United States. A "dimorphic" fungus, *H. capsulatum* exists as a saprophytic mold in soil and converts to the parasitic yeast form after inhalation. Only the yeasts secrete a calcium-binding protein (CBP) and can grow in calcium-limiting conditions. To probe the relation between calcium limitation and intracellular parasitism, we designed a strategy to disrupt *CBP1* in *H. capsulatum* using a telomeric linear plasmid and a two-step genetic selection. The resulting *cbp1* yeasts no longer grew when deprived of calcium, and they were also unable to destroy macrophages in vitro or proliferate in a mouse model of pulmonary infection.**

Histoplasma capsulatum is a pathogenic fungus that is a major cause of respiratory and systemic mycosis, especially in immunocompromised individuals (*1*). Histoplasmosis occurs worldwide but is endemic in the Mississippi and Ohio River valleys in the United States, where the organism thrives in soil in its mycelial (mold) form. As with most other dimorphic fungal pathogens, conversion to a unicellular haploid yeast form occurs after inhalation and exposure to the warmer temperature of the respiratory tract (*2*). There, *H. capsulatum* is readily engulfed by macrophages, in which the yeasts survive and proliferate within the normally hostile environment of phagolysosomes (*3*). The characteristics of this particular intracellular compartment are poorly understood, although we have previously demonstrated that *Histoplasma*-laden phagolysosomes fail to acidify (*4*). Studies with *Salmonella typhimurium*, which also survives within phagolysosomes of macrophages, have suggested that this compartment is low in Ca^{2+} concentration (*5*).

The latter observation may have particular relevance for *H. capsulatum*, as we have observed a major difference in calcium dependence between the saprophytic (mycelial) form and the parasitic (yeast) form. *Histoplasma capsulatum* yeasts are capable of growing in a calcium-deprived environment and secrete a 7.8-kD calcium-binding protein (CBP); in contrast, mycelial cultures do not secrete CBP and require calcium for growth (*6*). The CBP structural gene, *CBP1*, has been cloned and sequenced, and a potential calcium binding site is predicted from the secondary structure of CBP (*7*). Purified CBP has also been shown to increase the association of $^{45}CaCl_2$ with *H. capsulatum* yeasts after they have been transferred to low-calcium medium (*7*). To verify the functional role of CBP in calcium acquisition and/or virulence, we devised a generally applicable gene-disruption strategy for *Histoplasma*: Linear telomeric plasmids and a two-step ge-

Department of Molecular Microbiology, Campus Box 8230, Washington University School of Medicine, St. Louis, MO 63110, USA.

*To whom correspondence should be addressed. E-mail: goldman@borcim.wustl.edu